Ovonic Threshold Switching in Se-rich Ge_xSe_{1-x} Glasses from an Atomistic Point-of-View: the Crucial Role of the Metavalent Bonding Mechanism

Jean-Yves Raty* and Pierre Noé

Dr. J.Y. Raty [1,2] , Dr. Pierre Noé[2]
[1] FNRS, SPIN-CESAM, Université de Liège, 19 Allée du 6Août, 4000 Sart-Tilman, Belgium
[2] Univ. Grenoble Alpes, CEA, LETI, F-38000 Grenoble, France

E-mail: jyraty@uliege.be

Abstract

The Ovonic Threshold Switching (OTS) phenomenon, a unique discontinuity of conductivity upon electric-field application, has been observed in many chalcogenide glasses, some of which being presently used as selector elements in latest ultimate phase-change memory devices. In this work, *Ab Initio* Molecular Dynamics is used to simulate the structure of two prototypical glasses that have been shown to exhibit significantly different OTS properties and switching performance in OTS devices. The first glass, $Ge_{30}Se_{70}$ has a typical structure of connected Ge tetrahedra, whereas in the second $Ge_{30}Se_{70}$-based glass that contains antimony and nitrogen, the structure around Ge atoms is quite more complex. By the simulation of the excitation of electrons in the conduction band, slight modifications of the local order are shown to be sufficient to delocalize electronic states. The electron delocalization involving both Ge, Se (as well as Sb atoms in case of Sb-containing glass) ensures the percolation of conductive paths for electrons giving therefore to the excited material a metallic behavior. These conductive channels result from the local formation of 'metavalent' bonds [1, 2] in the amorphous structure as characterized geometrically and with associated Born effective charges.

1. **Introduction**

In the recent years, performant non-volatile though fast memories have been obtained thanks to the use of Phase-Change Materials (PCMs). These PCMs, most often found in a well-defined zone of the ternary Ge-Sb-Te phase diagram, have the ability to be switched between a conductive crystalline phase and a far more resistive amorphous phase using electrical pulses. For the RESET operation, an intense current pulse is flown onto the cell, which locally melts the PCM that crystallizes rapidly afterwards.

PCM memories are at origin of the birth of a new class of memory with so-called Storage Class Memory, a universal memory exhibiting a performance trade-off between the low latency of volatile dynamic random access memory (DRAM) and the non-volatility of flash memories. Besides, PCMs offers the opportunity to achieve ultra-high density memories thanks to 3D integration in resistive crossbar arrays, in which the memory cells are connected together in parallel along wordlines and bitlines. One of the challenges for PCM-based crossbar arrays is to insert the PCM memory element in an architecture which enables to apply high currents at moderate voltage on a given cell with no, or very limited, leakage current on the adjacent cells to prevent undesired programming. This was recently achieved in the 3D crossbar architecture of the Optane[TM] memory technology thanks to the adjunction of a so-called selector element to each PCM cell[3, 4]. This selector consists of a glassy chalcogenide that exhibits Ovonic Threshold Switching (OTS) at moderate voltage as well as a leakage current that is orders of magnitude smaller when un-switched.

This OTS phenomenon has been known for several decades [5] and has been observed in many chalcogenide glasses based on Se and Te elements. It consists in the reversible transition between a highly resistive (OFF state) and a conductive state (ON state) when the voltage applied on the OTS glass exceeds a critical threshold value, V_{th}. When the current is reduced below the holding current density, J_h, the selector recovers its high resistance state [6, 7].

Several models have been presented that describe the effect as due to the activation of hopping of electrons between trapped states present in the gap or band tails of the glasses[8, 9], a thermally assisted mechanism[10, 11] or to the formation of an unstable conductive filament within the amorphous material upon high-electric field application[12]. Most recently, a band tail model has been proposed in which Ge-Ge bonds are proposed to be at origin of conduction band tail states that lead to the non-linear conduction of Ge-rich Ge_xSe_{1-x} OTS materials[13]

However, an atomistic description of the process is still lacking. In this work, we present the results of *ab initio* molecular dynamics simulations performed on two different OTS glasses upon electronic excitation: $Ge_{30}Se_{70}$ (GS) and $Ge_{23}Se_{53}Sb_{19}N_5$ (GSSN). The choice of these two specific compositions has been dictated by the fact that Sb and N-doped Ge30Se70 glasses showed the ideal trade-off in terms of OTS properties, while being free of Arsenic. Indeed, such glasses exhibit a high stability against crystallization thanks to the introduction of nitrogen, a low Vth resulting from reduced bandgap due to Sb incorporation and limited subthreshold currents due to removal of Sb-Sb and Ge-Sb homopolar/wrongs bonds by N doping [14]. They were recently successfully integrated in state-of-the-art OTS devices [7].

2. Simulation method

The molecular dynamics simulations were performed within the Density Functional Theory framework, using the Vienna Ab Initio Software Package[15] code with PAW[16] potentials and GGA-PBE exchange correlation functional[17]. The 240 atoms initial amorphous models with atomic compositions $Ge_{72}Se_{168}$ and $Ge_{55}Se_{127}Sb_{46}N_{12}$ were prepared by the melt-and-quench approach using a Nosé thermostat. A first randomization is performed at 3000K, then the system is thermalized at 1000 K before being quenched to 800 K, 600 K and finally 300 K for a total simulation time exceeding 100 ps. The density was set to the experimental value. The time step was set to 3 fs for GS, but was reduced to 1 fs for GSSN. Five independent trajectories were simulated for each system and the results shown here are obtained by averaging over the last 5

ps of the simulation. To mimic the effect of an electric field, we forced a one-half occupation of electronic states at the top of the valence band, and at the bottom of the conduction band. The number of such states was defined by including those conduction states whose energy is less than 1 eV above the top of the valence states. This scheme has the advantage of maintaining a fixed number of excited electrons during the dynamics whereas conventional free energy density functional simulation would be more adapted to simulate the effect of optical excitation, as done for instance in amorphous Se [18] . A review of the various models for optical excitations effects in glasses can be found in Ref.[19]. It should be noted that in the experiments, OTS is observed typically for a voltage of about 3 volts applied to a 25nm thick film, which makes a direct simulation out of reach of current ab initio techniques. The temperature of ions was set to 300 K. The excitation was forced for 30 ps before the system was annealed at 300 K without excitation for another 30 ps. The DoS were computed using the HSE06 hybrid functional[20] in order to improve the description of the electronic gap.

To relate the changes in electronic structure generated by the excitation with local geometric details, we computed the Born effective charge tensors for all atoms using Density Functional Perturbation Theory[21]. These effective charges, which express the response of local atomic charge to an electric field, are only defined for nonmetallic system. Therefore, we performed a few conjugate gradient (usually about 10 steps) relaxation steps of individual excited structures with semiconductor occupation of states until a gap of the order of 0.1 eV is observed and then computed Z* charges. In an actual system, Z* values would diverge upon closing the electronic gap. With our approach, the structures are very close to those in the excited states and the Z* values are an effective measure of the way electrons around individual atoms react to the electric field. Note that we did not include Grimme-like functionals to account for van der Waals interactions in our simulations as these are based on tabulated coefficients that were obtained by fitting polarizabilities in a set of reference molecules [22]. We show in the following that

effective charges (related to polarizabilities) significantly vary in our glassy systems making the use of such functional unreliable.

3. **Results**

Before detailing the effect of excitation on the glasses, it is worth mentioning that the two systems have very different structural characteristics in the initial melt-quenched state.[23-25] First, the GS glass topology is known to be essentially dictated by tetrahedral $GeSe_4$ motifs (Ge coordination equals 3.81 with 60% of tetrahedra) that are often corner- or even edge sharing (65 and 35% of all tetrahedra, respectively[26]), as it has been shown in the literature before. Homopolar Ge-Ge bonds are almost absent, whereas 30% of Se bonds are Se-Se (see **Table 1**). The GSSN glass structure obtained here has no literature counterpart and has an underlying network topology that differs strongly from GS. This difference comes from a higher coordination of Se atoms (see Table 1) but more importantly from the bonding angles (see **Figure 1**).

It is remarkable that although Ge atoms have a coordination number that is close to 4 in both glasses, the substitution of some Se atoms by Sb and N in GSSN strongly modifies the bonding angle distributions, that become peaked around 90°, with an additional peak appearing at high angle values. For Se, the higher coordination in GSSN goes with the quasi disappearance of homopolar Se-Se bonds that are predominantly replaced by Se – Sb bonds. Again, this favors bonding around 90 degrees. The glass topology is therefore dominated by octahedral motifs in GSSN, in the sense that all angle distributions are peaked around 90°.

It can also be noted that thanks to the overall coordination increase in GSSN, the network rigidity is reinforced, as it is explained in references[27, 28]. It was shown in the case of amorphous GeTe that such increase, in that case associated to doping with N[29], was improving the stability of the glass against crystallization, which would be redhibitory for a use as OTS material.

5

Now let us consider the OTS ability of these two glasses. The analysis of the electronic properties of the two glasses shows that these have gaps with very few defect states (not shown here).

Upon electronic excitation, it must be emphasized that no atomic diffusion is observed at 300 K, however structural variations are noticeable, and these are responsible for strong changes in electronic properties.

First, the changes in distances and coordination numbers are modest, as reported in Table 1. In both glasses, coordination numbers increase by less than 0.1 atom upon excitation for Se, Sb and N, only the Ge coordination increases substantially by 0.3 atom in GS and 0.23 atom in GSSN. To interpret these changes, we plotted the distributions of bonding angles in Figure 1. Most changes occur in the Se-Ge-Se (both in GS and GSSN) and Se-Se-Se angular distribution in GS. In these, the proportion of angles with values close to 90° is increasing upon excitation, which translates into the appearance of a shoulder in Se-Ge-Se and Se-Se-Se angles in GS, and in the decrease of the shoulder peaked around 109° in Se-Ge-Se angle for GSSN. An enhancement of the octahedral character of bonding around Sb atoms is also observable in the Se-Sb-Se angle in GSSN, with both peaks close to 90° and at high angles (>150°) having a slightly higher value upon excitation. Interestingly, these changes are quite reversible, the ‚octahedral order' tendency decreasing when excitation is cancelled.

The effect of these local changes in bonding angle onto the electronic density of states (DoS) is illustrated in **Figure 2** for GSSN (similar changes are observed for GS). To estimate the degree of localisation of the electronic states, we projected the wavefunction onto atomic orbitals and computed the Inverse Participation Ratio (IPR) from the projections coefficients (IPR). By construction, the IPR value is comprised between 0 and 1; the ideal value of 1 would be observed for a state that would be fully contained in a single atomic orbital, whereas the 0 value limit would be obtained for a state that would be equally distributed over all atomic orbitals of an infinite system. In our case, the limit value would be $1/(4N)$, as 4 atomic orbitals are

considered N atoms in the system. Before excitation, the localization of states is the strongest around the gap (maximum value of about 1/4.5). Upon excitation (1 eV), the gap closes at the Fermi energy and the localization of the states drops to reach ~1/23, value that is similar those of deeper p valence states. Instead, the excitation has produced a pseudo-gap 0.5eV above the Fermi level, with strongly localized states with a high IPR reaching 0.35. From these observations, we can guess that delocalized states have been created around E_F by the excitation, which is quite expected as we forced a metallic occupation of states.

To understand the mechanism behind this "metallization", it is necessary to relate the newly created metallic states with the small structural changes that are observed. The direct inspection of the states wavefunction gives only qualitative indications. Indeed, these metallic states are essentially spread over a rather large number of Ge, Se and Sb atoms. To be more specific, we chose to probe the electronic structure in a slightly different way, focusing on the response properties of the electronic cloud to an external electric field. As this is not achievable for a metallic state, we simply performed a few relaxation steps (typically 10 conjugate gradient steps) on the excited metallic structure, these steps producing minor structural changes but being sufficient to open a gap at E_F. The analysis of the atomic dynamical charge, the Born effective charge Z^*, can then give direct measure of the dynamical polarizability of bonds (which would diverge just before metallization). High values of these effective charges are thus observed for those bonds that create the metallic state upon excitation. The results are shown in **Figure 3**. The values plotted are the maximal (absolute) value of the Z^* tensor as a function of relevant interatomic distances. These distances are those that are most sensitive to the angular variations observed upon excitation, typically the 3rd neighbor's distance for Se, the 4th for Ge, and the 4th and 5th distances for Sb atoms (N atoms do not show any particular trend). As we observed an increased octahedral tendency, we computed in each case the number of pairs of (quasi) aligned bonds, these being defined as two bonds that do not deviate with each other by

more than 30 degrees. Indeed, Figure 3 indicates that upon excitation the degree of bond alignment globally increases for Ge and Se atoms in GS, and for Ge and Sb atoms in GSSN. First, looking at Ge atoms, we see that the degree of bond alignment substantially increases for those 4th neighbor bonds that have intermediate (around 3 Å) values. These bonds lengths are absent in tetrahedral Ge motifs and are observed in 4-fold octahedral Ge atoms (and observed in GeTe[30-33] and GeSbTe glasses[34-36]). We see that these bonds are at the origin of the metallization upon excitation, as their effective charge become strongly anomal (they diverge when the gap closes). Se atoms also participate tot the metallization mechanism in GS, but play a minor role in GSSN. In GS, an increase in bond alignment for Se is also observed for short to intermediate 3rd neighbors' distances, which are not observed in a simple tetrahedrally bonded network. In GSSN on the contrary, changes around Se atoms are weak, with no particular correlation between bond alignment or polarizability increase being noticed. The case of antimony is somehow different as the local order before excitation has already a pronounced octahedral character, with a coordination of about 4 and angular distributions peaked around 90° and towards 180° (see Figure 2). The degree of bond alignment is thus high, but still increases slightly upon excitation. Metallization is promoted when the 4th and 5th neighbor bond lengths are short and bond alignment high.

From these observations, we obtain a model for OTS switching at the level of interatomic bonds. Within both glasses, and without atomic diffusion, electronic excitation produces slight modifications in bond lengths, but angular changes with important implications on the electronic side. In the mostly tetrahedral GS amorphous network, the metallization comes from the less tetrahedral Ge atoms via the alignment of two bonds which have intermediate bond lengths (2.8 – 3 Å). A similar effect is observed in GSSN. In GS, Se atoms are mostly two-fold bonded, and metallization comes from a better alignment of bonds, observed when atoms are closer to a 3-fold coordination. The participation of both Ge and Se atoms ensures the percolation of conductive paths for the electrons. In GSSN, Se atoms appear to play a neutral

role, whereas Sb atoms have an increased octahedral character upon excitation, with shorter 5th interatomic distances, which add to the changes in the Ge atoms environment.

The common point to all atoms is that those bonds that delocalize upon excitation are those that are quasi-aligned and that are sufficiently short. For Ge and Se, this means successive bonds with lengths typically smaller than 3.1 Å, for Sb this is observed for 4th and 5th neighbor bonds lengths around 3.1 Å. Such geometries are observed in crystalline chalcogenides, such as GeTe[37] or GeSe ($Ge_{50}Se_{50}$), as well as in GeTe and GST amorphous phase-change materials. A recent investigation of a variety of crystalline materials has related this kind of geometries with specific properties, such as high effective charges, high dielectric constant and high anharmonicity.[1, 2] Actually those materials are close to being metallic, most of them being phase-change materials. The bonds have been qualified as metavalent and the associated materials properties linked with the fact that the bonds are close to half-filled. In crystalline GeTe, it was shown that the anomal increase of Z* appears with the shortening of the 4th (and 5th and 6th) neighbor distances with quasi-aligned bonds, whereas in crystalline GeSe, bond alignment is worse and 4th distances are proportionally longer, in consequence of which no Z* anomaly is observed.

In the present excited case, the excitation of GS and GSSN glasses is modifying the bond geometry so that they become partly filled and conductive by their alignment. We thus observe the appearance of the characteristics of metavalent bonds upon excitation.

This provides a quite general picture for the OTS switching mechanism in Ge-Se based glasses, picture that could possibly be extended to other chalcogenide glasses in the future.

Acknowledgements

Received: ((will be filled in by the editorial staff))
Revised: ((will be filled in by the editorial staff))
Published online: ((will be filled in by the editorial staff))

References

[1] M. Wuttig, V. L. Deringer, X. Gonze, C. Bichara, J.-Y. Raty, *Adv. Mater.* **2018**, *30,* 1803777.

[2] J.-Y. Raty, M. Schumacher, P. Golub, V. L. Deringer, C. Gatti, M. Wuttig, *Adv. Mater.* **2019**, *31,* 1806280.

[3] T. Kim, H. Choi, M. Kim, J. Yi, D. Kim, S. Cho, H. Lee, C. Hwang, E. R. Hwang, J. Song, S. Chae, Y. Chun, J. K. Kim, *Tech. Dig. - Int. Electron Devices Meet. IEDM 2018*, **2019**, 37.1.1.

[4] http://www.techinsights.com/about-techinsights/overview/blog/intel-3D-xpoint-memory-die-removed-from-intel-optane-pcm/

[5] S. R. Ovshinsky, *Phys. Rev. Lett.* **1968**, *21,* 1450.

[6] Noé, P., Vallée, C., Hippert, F., Fillot, F. & Raty, J.-Y., *Semicond. Sci. Technol.* **2018**, 33, 013002.

[7] Pierre Noé, Francesco d'Acapito, Jean-Baptiste Dory, Mathieu Bernard, Gabriele Navarro, Jean-Baptiste Jager, Jérôme Gaudin and Jean-Yves Raty*, in press*, Science Advances **2019** DOI: 10.1126/sciadv.aay2830.

[8] D. Ielmini, *Phys. Rev. B* **2008**, *78,* 035308.

[9] D. Ielmini, Y. Zhang, *J. Appl. Phys.* **2007**, *102,* 054517.

[10] A. Redaelli, A. Pirovano, A. Benvenuti, A. L. Lacaita, *J. Appl. Phys.* **2008**, *103,* 111101.

[11] M. L. Gallo, A. Athmanathan, D. Krebs, A. Sebastian, *J. Appl. Phys.* **2016**, *119,* 025704.

[12] I. Karpov, M. Mitra, D. Kau, G. Spadini, Y. A. Kryukov, V. G. Karpov, *Appl. Phys. Lett.* **2008**, *92,* 173501-173501.

[13] H. Li, J. Robertson, *Sci. Rep.* **2019**, *9,* 1867.

[14] A. Verdy, F. d'Acapito, J.B. Dory, G. Navarro, M. Bernard, and P. Noé, *Phys. Status Solidi RRL* **2019**, 1900548.

DOI: 10.1002/pssr.201900548"

[15] G. Kresse, J. Furthmüller, *Comput. Mater. Sci.* **1996**, *6,* 15.

[16] G. Kresse, D. Joubert, *Phys. Rev. B* **1999**, *59,* 1758.

[17] J. P. Perdew, K. Burke, M. Ernzerhof, *Phys. Rev. Lett.* **1996**, *77,* 3865.

[18] J.Hegedüs, K.Kohary, S.Kugler J. Phys. Chem. Solids **2007** 68, 1069.

[19] H. Fritzsche, Physica Status Solidi B **2009** 246, 1678

[20] A. V. Krukau, O. A. Vydrov, A. F. Izmaylov, G. E. Scuseria, *J. Chem. Phys.* **2006**, *125,* 224106.

[21] X. Gonze, C. Lee, *Phys. Rev. B* **1997**, *55,* 10355.

[22] S. Grimme, J. Antony, S. Ehrlich, and H. Krieg, *J. Chem. Phys*. **2010**, 132, 154104.

[23] P. Salmon, *J Non-Cryst Solids* **2007**, *353,* 2959-2974

 [24] C. Massobrio, A. Pasquarello, *J Phys Condens Matter* **2007**, *19,* 415111.

[25] M. Micoulaut, A. Kachmar, M. Bauchy, S. Le Roux, C. Massobrio, M. Boero, *Phys. Rev. B* **2013**, *88,*

[26] S. Le Roux, P. Jund, *Comput. Mater. Sci.* **2010**, *49,* 70.

[27] M. Micoulaut, J.-Y. Raty, C. Otjacques, C. Bichara, *Phys. Rev. B* **2010**, *81,* 174206.

[28] A. Piarristeguy, A. Pradel, J.-Y. Raty, *MRS Bulletin* **2017**, *42,* 45.

[29] J.-Y. Raty, P. Noé, G. Ghezzi, S. Maîtrejean, C. Bichara, F. Hippert, *Phys. Rev. B* **2013**, *88,* 014203.

[30] J.-Y. Raty, *Phys. Status Solidi RRL* **2019**, *13,* 1800590.

[31] T. H. Lee, S. R. Elliott, *Adv. Mater.* **2017**, *29,* 1700814.

[32] F. Zipoli, D. Krebs, A. Curioni, *Phys. Rev. B* **2016**, *93,* 115201.

[33] S. Gabardi, S. Caravati, G. Sosso, J. Behler, M. Bernasconi, *Phys. Rev. B* **2015**, *92,* 054201.

[34] F. C. Mocanu, K. Konstantinou, T. H. Lee, N. Bernstein, V. L. Deringer, G. Csányi, S. R. Elliott, *J. Phys. Chem. B* **2018**,

[35] S. Caravati, M. Bernasconi, T. D. Kühne, M. Krack, M. Parrinello, , *J Phys Condens Mater* **2009**, *21,* 255501.

[36] C. Qiao, Y. Guo, F. Dong, J. Wang, H. Shen, S. Wang, M. Xu, X. Miao, Y. Zheng, R. Zhang, *J. Mater. Chem. C* **2018**, *6, 5001.

[37] B. Huang, J. Robertson, *Phys. Rev. B* **2010**, *81,* 081204.

Figure 1. Principal bond angle distributions in amorphous GS and GSSN in their initial melt-quenched states (black lines), in the excited state (red lines) and after recovery (blue lines). Top panel: angular distributions for Ge and Sb. Se-Ge-Se angles in GS and GSSN with plain lines, Se-Sb-Se with dashed lines. Central panel: all bond angle distributions around Se atoms in GS. Bottom panel: main distributions of Se-centered angles in GSSN. Dashed lines have been draw at 90° and 109°. Representative environments are shown as insets for Ge in GS and GSSN, anf for Sb in GSSN (blue : Ge; green : Se; pink : Sb)
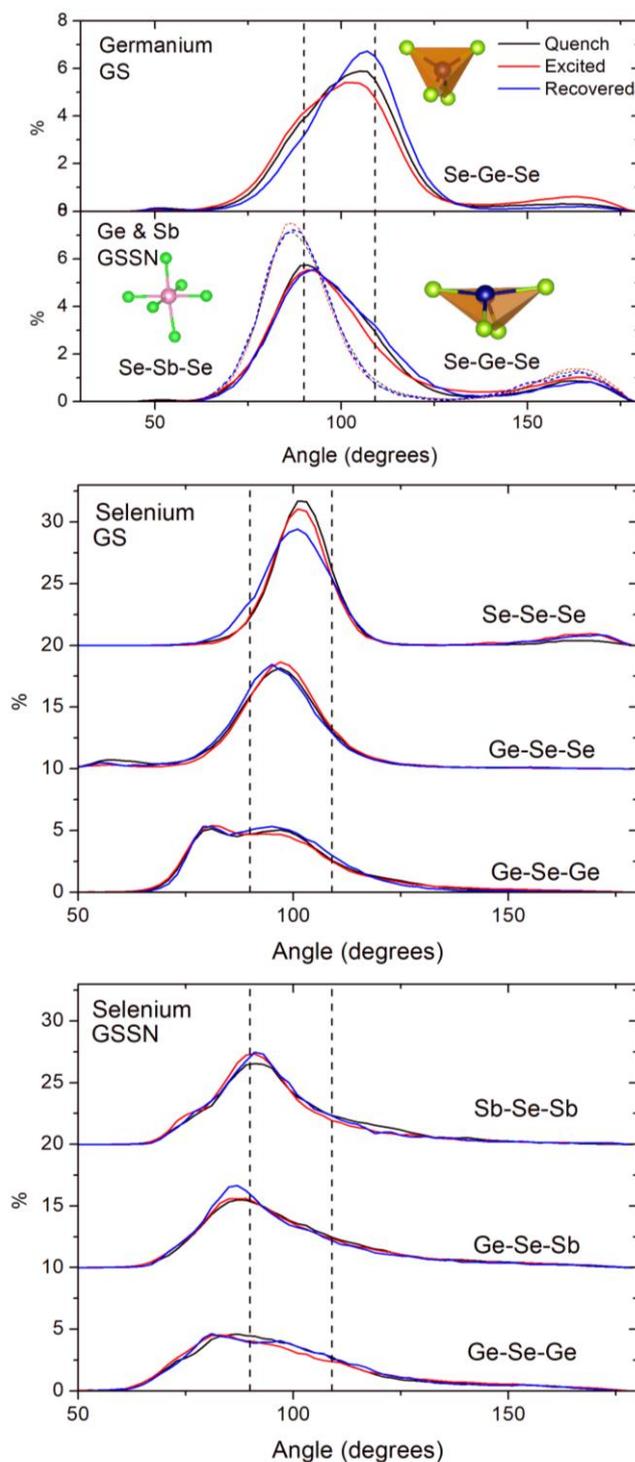
Figure 2. Density of electronic states and localization of states around the Fermi energy for the GSSN glass in the initial melt-quenched state (top panel) and during excitation (bottom panel). The densities of states (DoS) are computed with the HSE06 hybrid functional and a 0.1 eV smearing (Gamma point only). The inverse participation ratio (IPR) are plotted as histograms that are obtained by averaging IPR (0.1 eV bins). The dashed region is 0.2 eV wide and centered on the Fermi energy in both case (same height).
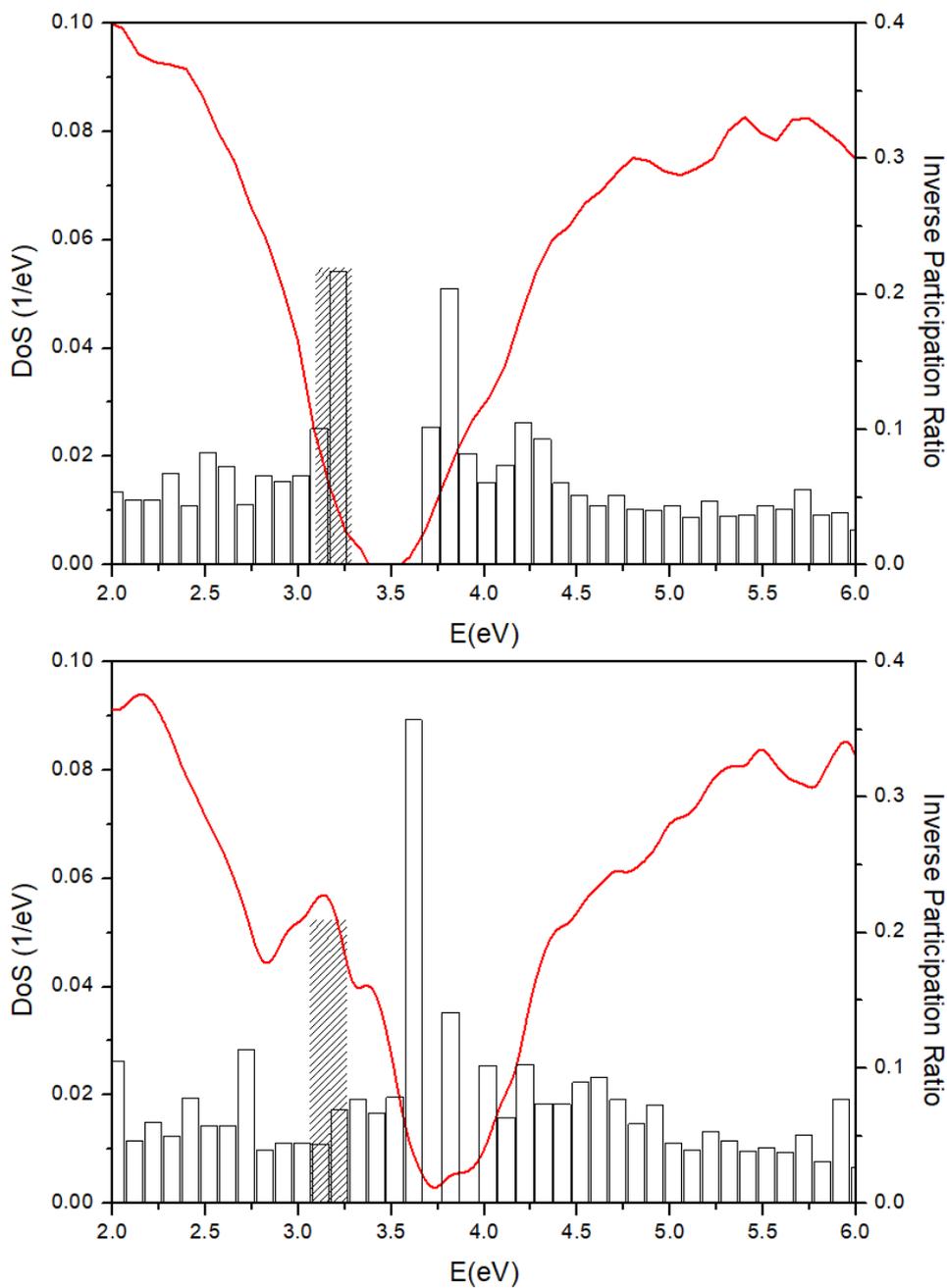
Figure 3. Illustration of the effect of electronic excitation onto the degree of bond alignment and on the bond polarizability. The degree of alignment (number of bond pairs that do not deviate by more than 30°) is plotted per atom and as a function of selected interatomic distances. The initial melt-quenched results are shown with empty symbols; the excited state values with filled symbols. The color code is given by the absolute maximal value of the Born effective charge. The top two panels show the results for Ge and Se atoms in GS. The relevant distances are the 4th (d4) and 3rd (d3) neighbor's ones, respectively. The insert show schematic representations of corresponding local geometries. The bottom four panels concern GSSN, with Ge (d4), Se (d3) and two panels for Sb, as a function of d4 and d5, respectively.

WILEY-VCH
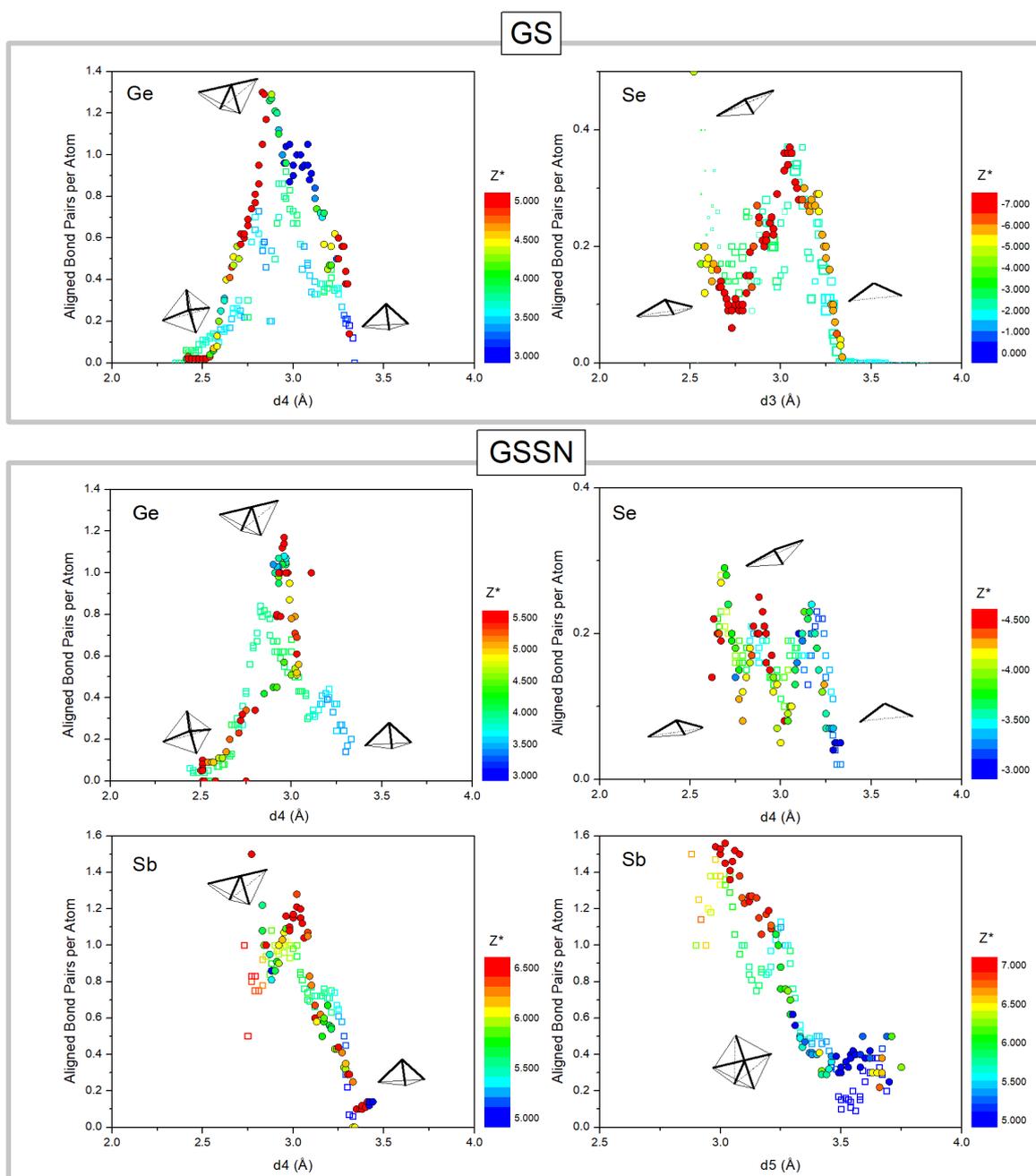
Table 1. Total coordination numbers (CN_{Total}) and projected partial coordination numbers (N) of Ge, Se, Sb and N atoms for GS and GSSN glasses in their various states: initial melt quenched, in the excited state and after recovery. The coordination numbers are obtained by integration of the first peak of the corresponding partial pair correlation function up to its first minimum.

		System	
		$Ge_{72}Se_{168}$	**$Ge_{55}Se_{127}Sb_{46}N_{12}$**
Element	Phase	CN_{Total} (N_{Ge} + N_{Se})	CN_{Total} (N_{Ge} + N_{Se} + N_{Sb} + N_{N})
Ge	Melt Quenched	3.81 (0.10 + 3.71)	3.93 (0.10 + 3.23 + 0.10 + 0.40)
	Excited	4.11 (0.09 + 4.02)	4.16 (0.13 + 3.55 + 0.08 + 0.40)
	Recovered	3.84 (0.12 +3.72)	3.95 (0.16 + 3.31 + 0.09 + 0.39)
Se	Melt Quenched	2.27 (1.59 + 0.68)	2.69 (1.40 + 0.14 + 1.14 + 0.01)
	Excited	2.33 (1.72 + 0.61)	2.76 (1.54 + 0.05 + 1.16 + 0.01)
	Recovered	2.22 (1.59 + 0.62)	2.62 (1.43 + 0.04 +1.13 + 0.01)
Sb	Melt Quenched		3.64 (0.12 + 3.15 + 0.03 + 0.35)
	Excited		3.70 (0.09 + 3.20 + 0.07 + 0.34)
	Recovered		3.62 (0.10 + 3.13 + 0.04 + 0.34)
N	Melt Quenched		3.30 (1.83 + 0.14 + 1.33 + 0.00)
	Excited		3.28 (1.82 + 0.14 + 1.32 + 0.00)
	Recovered		3.24 (1.80 + 0.14 + 1.30 + 0.00)

The effect of electronic excitation on two glasses exhibiting Ovonic Threshold Switching is studied by *ab initio* molecular dynamics. The glasses are shown to undergo modifications in bond angle distributions upon excitation. The modified bonds are better aligned and exhibit anomalous Born effective charge values. These are at the origin of the conductivity increase during Ovonic Threshold Switching.

Ovonic Threshold Switching

Jean-Yves Raty* and Pierre Noé

Ovonic Threshold Switching in Se-rich Ge$_x$Se$_{1-x}$ Glasses from an Atomistic Point-of-View: the Crucial Role of the Metavalent Bonding Mechanism